Title

Design of phase-shifted hybrid silicon distributed feedback lasers

Journal

Optics Express, 19(10)

Authors

Srinivasan, Sudharsanan
Fang, Alexander W
Liang, Di
et al.

Publication Date

2011-05-09

Peer reviewed

Design of phase-shifted hybrid silicon distributed feedback lasers

Sudharsanan Srinivasan,[1,*] Alexander W. Fang,[2] Di Liang,[1] Jon Peters,[1] Bryan Kaye,[1] and John E. Bowers[1]

[1]*Department of Electrical and Computer Engineering, University of California, Santa Barbara, CA 93106, USA*
[2]*Aurrion LLC, 130 Robin Hill Road, Goleta, CA 93117, USA.*
**sudhas@ece.ucsb.edu*

Abstract: We present data on the design and performance analysis of phase shifted distributed feedback (DFB) lasers on the hybrid silicon platform. The lasing wavelength for various input currents and temperatures, for devices with standard quarter-wavelength, 60 μm and 120 μm-long phase shift are compared for mode stability and output power. The pros and cons of including a large phase shift region in the grating design are analyzed.

OCIS codes: (140.3490) Lasers, distributed-feedback; (050.5080) Phase shift.

References and links

1. D. A. B. Miller, "Device requirements for optical interconnects to silicon chips," Proc. IEEE **97**(7), 1166–1185 (2009).
2. D. Liang and J. E. Bowers, "Recent progress in lasers on silicon," Nat. Photonics **4**(8), 511–517 (2010).
3. G. Morthier and P. Vankwikelberge, *Handbook of Distributed Feedback Laser Diodes* (Artech House, Inc., 1997), Chaps. 10 and 11.
4. A. W. Fang, E. Lively, Y. Kuo, D. Liang, and J. Bowers, "Distributed Feedback Silicon Evanescent Laser," in *National Fiber Optic Engineers Conference*, OSA Technical Digest (CD) (Optical Society of America, 2008), paper PDP15.
5. H. Ghafouri-Shiraz, *Distributed Feedback Laser Diodes and Optical Tunable Filters* (Wiley, 2003), Chaps. 3 and 5.
6. W. Alexander, Fang, "Silicon evanescent lasers," Ph.D. dissertation (Dept. of Elect. and Comp. Eng., Univ. of California, Santa Barbara, CA, 2008), pp. 104–105.
7. M. N. Sysak, H. Park, A. W. Fang, J. E. Bowers, R. Jones, O. Cohen, O. Raday, and M. J. Paniccia, "Experimental and theoretical thermal analysis of a hybrid silicon evanescent Laser," Opt. Express **15**(23), 15041–15046 (2007).

1. Introduction

Optical interconnects to and on silicon chips are necessary to address the issues of increasing power consumption and limited communication bandwidth faced by conventional electrical interconnects [1]. Wafer-bonding compound semiconductors to SOI substrates, combines the superior gain characteristics of compound semiconductors with the superior passive waveguide characteristics of silicon. Laser diodes fabricated on this hybrid platform make good light sources, which are useful for optical interconnects on silicon [2]. Distributed-feedback (DFB) lasers, useful because of its single longitudinal mode output and lithographically-defined cavity length, can produce milliwatts of output power with relatively low threshold currents, making them attractive candidates for on-chip light sources [3]. Earlier, Fang et al. successfully designed and fabricated a quarter-wave shifted DFB laser structure on the hybrid silicon platform [4]. Figure 1 shows the schematic longitudinal cross section of a hybrid DFB silicon laser. A standard DFB laser, without phase-shifts, relies on perturbing reflections to destroy the degeneracy of the two modes on either side of the Bragg wavelength. A single quarter-wave shifted DFB design eliminates the degeneracy and becomes resonant at the Bragg wavelength. However, the intense electric field concentrated at the phase shifted region of the cavity limits its performance primarily because of spatial hole burning [5].

#140211 - $15.00 USD Received 3 Jan 2011; revised 25 Feb 2011; accepted 28 Feb 2011; published 27 Apr 2011

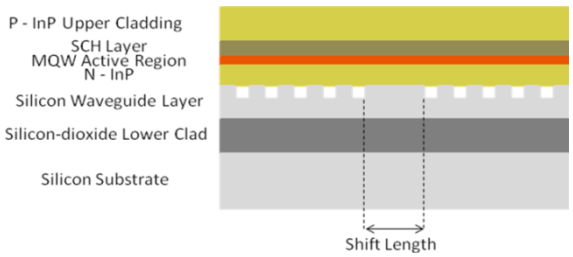

Fig. 1. Schematic of a symmetric phase-shifted DFB silicon laser.

In Section 2, we discuss the design and fabrication of the DFB lasers with different phase shift lengths. The theoretical and experimental threshold current and maximum power for the relevant devices is studied in Section 3. In Section 4, we analyze the spectral data to discuss mode stability and in Section 5, devices are compared from a thermal performance perspective.

2. Device design and fabrication

The devices were fabricated using the same procedure as in Ref [4]. The rectangular surface corrugations in this work are made on silicon, which enables us to have any form of grating structure with relatively low tolerance on dimensions because of advanced high-resolution CMOS lithography tools. The grating pitch is 238 nm and the stop band is designed around 1600 nm. Figure 2 shows an image of a processed hybrid silicon chip which contains 36 DFB laser designs distributed among 300 devices with a laser yield of over 95%.

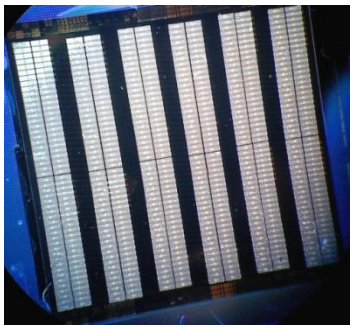

Fig. 2. Hybrid silicon chip showing 300 DFB lasers with on-chip photodetectors.

The coupling coefficient, κ, of the grating was designed for 250 cm^{-1}; this is large compared to gratings on passive silicon rib waveguides of similar dimension since the index difference between air and silicon is quite large and the index perturbation is located nearer to the center of the optical mode [6]. The κL product, where L is the length of the grating, is varied by changing L. In this paper, we compare the performance of eight designs, primarily distinguished by the phase-shift length introduced at the center of the grating (see Fig. 3). Long grating lengths were used in the DFB lasers of an earlier generation to minimize the negative effects of device heating, which lead to poor power extraction and low differential quantum efficiency. The goal of this paper is to find the effects of changing the phase-shift length and grating length on output power and mode stability. Two on-chip hybrid silicon photodetectors are integrated to detect the output power from both sides. We assume a responsivity of 1 A/W to conservatively estimate the device output power.

#140211 - $15.00 USD Received 3 Jan 2011; revised 25 Feb 2011; accepted 28 Feb 2011; published 27 Apr 2011

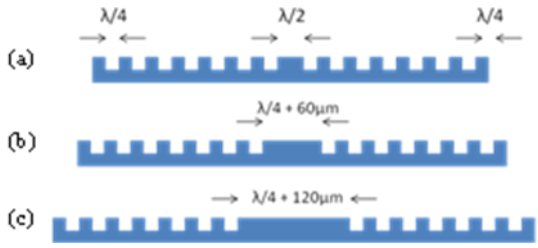

Fig. 3. Grating structures with phase-shift lengths equal to (a) one quarter wavelength (λ_0 = 1600 nm), (b) 60 μm, and (c) 120 μm.

3. Threshold current and maximum output power

Devices with III-V junction side up sit on a copper stage whose temperature is actively controlled during characterization. The stage temperature (T) was kept constant at 20 °C for all the measurements. Figure 4 shows a typical L-I-V curve for one of the DFB laser designs under cw operation. The total cavity length is 240 μm with 120 μm long phase-shift region, resulting in κL = 3. The series resistance for all devices lie between 20 Ω and 35 Ω.

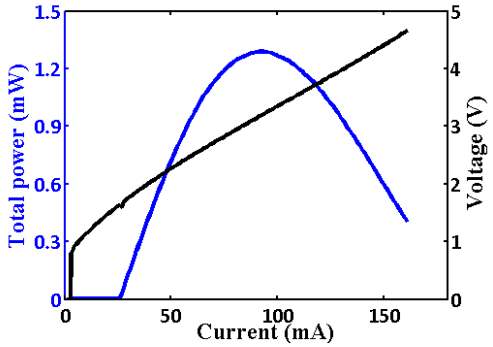

Fig. 4. L-I-V curve for a DFB laser with 120 μm long phase-shift and κL = 3. The total device length is 240 μm.

Figure 5 shows the experimental values of threshold current and maximum output power versus the grating coupling coefficient-grating length product, κL, alongside the theoretical curves. The error bars indicate the full range of measured values from various positions on the chip. We expect the threshold and output power to vary as described in Eqs. (1) and (2) respectively,

$$I_{th} = I_{th0} e^{(Z_T(P_D - P_{out}) + T)/T_0} \tag{1}$$

$$P_{out} = \eta_i \left(\frac{\alpha_m}{\langle \alpha_i \rangle + \alpha_m} \right) \left(\frac{h\nu}{q} \right) e^{\left(-(Z_T(P_D - P_{out}) + T)/T_1 \right)} (I - I_{th}) \tag{2}$$

where h, ν, q, $\langle \alpha_i \rangle$, α_m, η_i, and Z_T are Planck's constant, photon frequency, elementary charge, average internal modal loss, mirror loss, injection efficiency, and thermal impedance respectively. T_0 = 51 K, T_1 = 100 K, Z_L = 3.6975 (°K.cm)/W and $Z_T = Z_L/L_{tot}$ are obtained experimentally [7]. L_{tot} is the length of the gain region which is the sum of grating length and phase-shift length in our case. The values of internal quantum efficiency (ηi) and internal loss ($<\alpha i>$) extracted from fitting the experimental data to theory are 0.39 and 11 cm^{-1} respectively. We assume a logarithmic dependence of gain on carrier density and the material gain and transparency carrier density used in the relation are g_0 = 966 cm^{-1} and N_{tr} = 1.86 ×

#140211 - $15.00 USD Received 3 Jan 2011; revised 25 Feb 2011; accepted 28 Feb 2011; published 27 Apr 2011

10^{18} cm^{-3}. Both theoretical and experimental data show that the threshold decreases to a minimum value and then grows with reducing device length, L_{tot}, due to changes in mirror loss and average internal model loss. Similarly, the output power increases at the optimum value and then falls off. As the length of the phase shift region increases, the minimum threshold current in Fig. 5(a) moves to higher value and lower κL. The reason is twofold: First, threshold current density remains constant, so longer phase-shift lengths result in a longer cavity, and subsequently higher threshold current. Second, for a smaller κL, shorter device length leads to higher thermal impedance and hence a higher threshold current (Eq. (1)), as is confirmed by the experimental data.

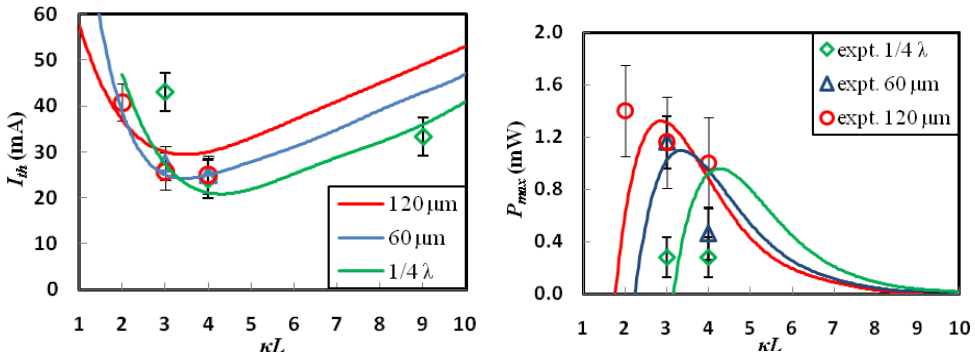

Fig. 5. Threshold current (a) and maximum output power (b) plotted against κL for three phase-shift lengths, one quarter wavelength (green line and diamonds), 60 μm (blue line and triangles) and 120 μm (red line and circles).

Using only the data from Fig. 5, large phase-shift lengths and lower κL products seem to have high power extraction. This is largely due to reduced device thermal impedance (Eq. (2)). However, we do not know the mode stability and side mode suppression ratio (SMSR) of these lasers which is important for interconnect operation given the relatively harsh conditions on the silicon chip.

4. Spectral Analysis

The devices were diced and polished on one side to obtain the spectrum. The bandwidth of the grating is roughly constant at about 10 nm due to constant κ. Resolution bandwidth and sensitivity of the optical spectrum analyzer were set to 0.1 nm and −90 dBm respectively. Figure 6(a) shows the theoretical threshold modal gain condition, $(\Gamma g_{th} - \alpha_i)L$, for the cavity modes in a quarter-wave shifted DFB laser. The cavity is resonant at the Bragg wavelength. The higher order modes are symmetric about the null of detuning parameter, $\delta L = (\tilde{\beta} - \beta_0)L$ where $\tilde{\beta}$ and β_0 are the average propagation constant and Bragg wavenumber respectively.

Since the first higher order modes for κL = 3 and 4 require sufficiently higher gain than the fundamental mode, the lasers are able to operate at the single longitudinal mode stably with roughly 40 dB SMSR (Fig. 6(b)). However, any increase in grating length brings down the threshold modal gain for the higher order modes, leading to easier modal competition, and subsequently multiple longitudinal modes lasing.

#140211 - $15.00 USD Received 3 Jan 2011; revised 25 Feb 2011; accepted 28 Feb 2011; published 27 Apr 2011

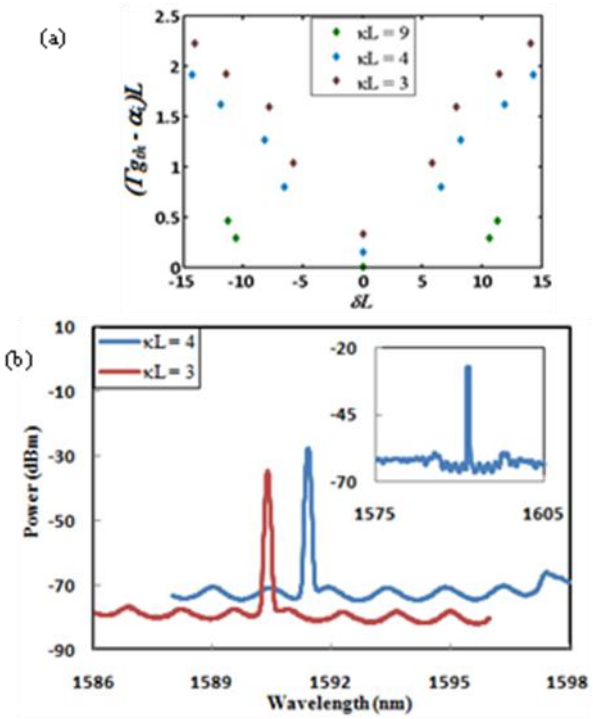

Fig. 6. (a) The solutions to threshold modal gain condition in a quarter-wave shifted DFB laser for cavity modes near the Bragg wavelength. (b) The spectrum at 70 mA and 90 mA injection current for devices with κL = 3 and 4 respectively. Inset: The cw lasing spectrum over 30nm showing single mode lasing.

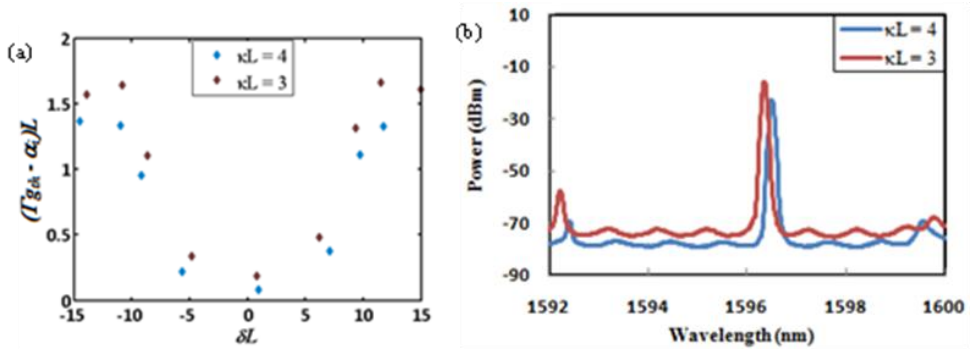

Fig. 7. (a) The solutions to threshold modal gain condition in a DFB laser, with 60 μm phase-shift length, for cavity modes near the Bragg wavelength. (b) The spectrum at 90 mA and 100 mA injection current for devices with κL = 3 and 4 respectively.

The theoretical threshold modal gain condition for the cavity modes in a 60 μm phase-shift length laser is shown in Fig. 7(a). The grating is no longer resonant at the Bragg wavelength. The difference in modal gain between the zero order mode and the first higher order mode to its left, is significantly less compared to the quarter-wave shifted case in Fig. 6(a). This reflects itself in the spectrum as an obvious side-mode close to the edge of the grating bandwidth.

The situation, however, worsens when the phase-shift length is 120 μm. Figure 8(a) shows five modes around the Bragg wavelength that require nearly the same threshold modal gain for lazing. It results in simultaneous lasing of several modes as shown in Fig. 8(b). In such

#140211 - $15.00 USD Received 3 Jan 2011; revised 25 Feb 2011; accepted 28 Feb 2011; published 27 Apr 2011

cases, the primary lasing mode is determined by the material gain profile, and we observe mode hopping as material gain profile shifts with higher injection current. The SMSR falls below 40 dB. We note that the spacing between the modes is ~2.5 nm, half as much as what we see in Fig. 6(b). This agrees well with a simple calculation using a Fabry-Perot cavity that is as long as the phase-shift length.

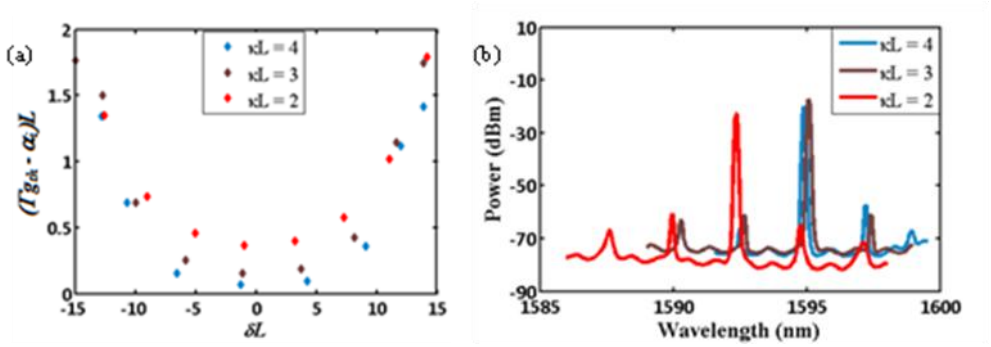

Fig. 8. (a) The solutions to threshold modal gain condition in a DFB laser, with 120 μm phase-shift length, for cavity modes near the Bragg wavelength. (b) The spectrum at 90 mA injection current for devices with κL = 2, 3 and 4.

5. Thermal Impedance

The thermal performance of silicon evanescent lasers is currently limited by heat extraction from the active region, due to the presence of silicon dioxide lower cladding in the SOI substrate [7]. This limits the maximum lasing temperature and degrades the device performance. The ratio of change in lasing wavelength to the change in input electrical power ($d\lambda/dP_{elec}$) and change in stage temperature ($d\lambda/dT$), for the eight designs under cw operation are plotted in Figs. 9(a) and (b) respectively. The data points in Fig. 9(b) are concentrated around the value of 0.1nm/°C for all designs. Thus the value of $d\lambda/dP_{elec}$ is a good tracking point for the thermal impedance of the device.

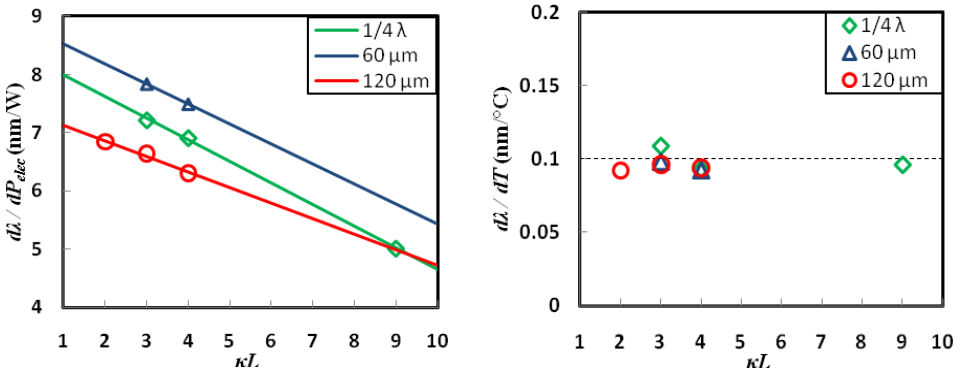

Fig. 9. (a) The ratio of change in lasing wavelength to change in input electrical power for different laser designs in cw operation. The lines are a linear fit to the data points. (b) The ratio of change in lasing wavelength to change in stage temperature for the same designs.

Since the electric field intensity peaks in the phase shift region much of the heat is generated here in the laser. Thermal impedance of the device scales inversely with device length. Hence, we expect the thermal impedance of the lasers with phase-shift length of 60 μm and 120 μm not to increase significantly with decrease in grating length when compared to the quarter-wave shifted laser. The slopes in Fig. 9(a) corresponding to phase-shift lengths of ¼ λ, 60 μm and 120 μm are 0.372, 0.344 and 0.268 respectively, consistent with this hypothesis.

#140211 - $15.00 USD Received 3 Jan 2011; revised 25 Feb 2011; accepted 28 Feb 2011; published 27 Apr 2011

6. Conclusions

We designed and studied eight symmetric phase-shifted DFB lasers on a hybrid silicon platform. The effects of incorporating long phase-shift lengths are studied from device, electrical, optical, spectral and thermal perspectives. Phase-shift lengths much longer than one quarter wavelength can provide good power extraction, while keeping the thermal impedance of the device low. However, very long phase-shift lengths lead to mode instability and degraded SMSR. Optimal designs are determined by the application requirement.

Acknowledgments

The authors would like to thank Hui-Wen Chen and Yongbo Tang for valuable discussions and fabrication assistance, and NSF funded NNIN fabrication facility at the University of California, Santa Barbara. This research was supported by the DARPA CIPhER project.

#140211 - $15.00 USD Received 3 Jan 2011; revised 25 Feb 2011; accepted 28 Feb 2011; published 27 Apr 2011